THE JOURNAL OF PHYSICAL CHEMISTRY LETTERS
A JOURNAL OF THE AMERICAN CHEMICAL SOCIETY

pubs.acs.org/JPCL

Letter

Thermoelectric Properties of Benzothieno-Benzothiophene Self-Assembled Monolayers in Molecular Junctions

Sergio Gonzalez-Casal, Rémy Jouclas, Imane Arbouch, Yves Henri Geerts, Colin van Dyck, Jérôme Cornil, and Dominique Vuillaume*

Cite This: J. Phys. Chem. Lett. 2024, 15, 11593−11600

Read Online

ACCESS | Metrics & More | Article Recommendations | Supporting Information

ABSTRACT: We report a combined experimental (C-AFM and SThM) and theoretical (DFT) study of the thermoelectric properties of molecular junctions made of self-assembled monolayers on Au of thiolated benzothieno-benzothiophene (BTBT) and alkylated BTBT derivatives (C8-BTBT-C8). We measure the thermal conductance per molecule at 15 and 8.8 pW/K, respectively, among the lowest values for molecular junctions so far reported (10−50 pW/K). The lower thermal conductance for C_8-BTBT-C_8 is consistent with two interfacial thermal resistances introduced by the alkyl chains, which reduce the phononic thermal transport in the molecular junction. The Seebeck coefficients are 36 and 245 μV/K, respectively, the latter due to the weak coupling of the core BTBT with the electrodes. We deduce a thermoelectric figure of merit ZT up to $\approx 10^{-4}$ for the BTBT molecular junctions at 300 K, on a par with the values reported for archetype molecular junctions (oligo(phenylene ethynylene) derivatives).

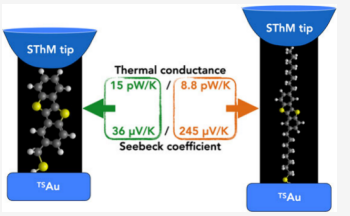

Molecular junctions (MJs) have been suggested as efficient thermoelectric devices at the nanoscale.[1] Due to their nanoscopic scale and quantum behavior, the classical Fourier's law is broken down,[2] and among other deviations, the thermal conductivity of MJs is size-dependent or equivalently the thermal conductance no longer scales as $1/L$ (with L the molecule length) but is almost constant or varies as $1/L^{0.64}$.[3−9] More research is definitely required to explore molecular thermoelectricity and to develop efficient thermal management strategies for molecular nanodevices.[10] The complete study of the thermoelectric properties of MJs requires measuring the electrical conductance G_{el}, the Seebeck coefficient S (thermopower), and the thermal conductance G_{th} (equivalently, the conductances translate to the electrical conductivity σ and to the thermal conductivity κ considering the *ad-hoc* geometrical factors of the measured devices).[11] The experimental determination of the thermal conductance of molecular junctions is relatively scarce compared to the first two factors (see reviews in refs 9, 12, 13), especially considering studies at the nanoscale in devices featuring self-assembled monolayers (SAMs) or single molecules. Moreover, the results reported so far concern only MJs based on alkanethiols and oligo-(phenylene ethynylene) (OPE). Meier et al.[7] studied the thermal conductance of SAM-based MJs (Au-alkanethiol-Au) using scanning thermal microscopy (SThM) and reported a thermal conductance (per molecule) in the range 10−30 pW/K decreasing as $L^{0.64}$ for alkyl chain lengths between 2 and 18 carbon atoms. More recently, SThM-based experiments on single molecule MJs measured a thermal conductance in the range of 15−30 pW/K for Au-alkanedithiol-Au (almost constant for 2 to 10 carbon atoms),[8] ≈37 pW/K (for 8 carbon atoms),[14] and ≈23−24 pW/K for OPE-based MJs.[11,14]

Here, we report the thermoelectric properties of SAM-based MJs made of benzothieno-benzothiophene (BTBT) thiolated derivatives. BTBT derivatives are interesting molecules for several applications in electronics such as transistors owing to their high charge mobility.[15,16] We previously compared the thermal conductivity (measured by SThM) of polycrystalline thin films (40−400 nm) of BTBT and alkylated BTBT derivatives (octyl chains at the α and ω positions of the BTBT core, C_8-BTBT-C_8).[17] From a combined SThM and computational study, we unveiled that the thermal conductivity of the BTBT films is larger than that of the alkylated BTBT (0.63 W m^{-1} K^{-1} vs 0.25 W m^{-1} K^{-1}) because the alkyl chains strongly localize the phonon modes in the BTBT layers. In the present work, we synthesized the thiol functionalized derivatives of the same molecules to form SAMs on Au electrodes and characterized the thermal and electrical conductances of these SAM-based MJs by SThM and conductive-AFM (C-AFM). The thermal conductivity of the BTBT SAM is measured at $\kappa_{SAM(BTBT)}$ = 0.46 ± 0.27 W m^{-1} K^{-1} and $\kappa_{SAM(C8\text{-}BTBT\text{-}C8)}$ = 0.27 ± 0.16 W m^{-1} K^{-1} (*i.e.*, a thermal conductance of the SAMs $G_{th,SAM(BTBT)}$ = 37 ± 21 nW/K and $G_{th,SAM(C8\text{-}BTBT\text{-}C8)}$ = 22 ± 13 nW/K. From these values, we estimated the thermal conductance per molecule at 15 pW/K and 8.8 pW/K, respectively, which is slightly lower than that

Received: September 20, 2024
Revised: November 7, 2024
Accepted: November 8, 2024
Published: November 11, 2024

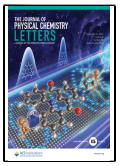

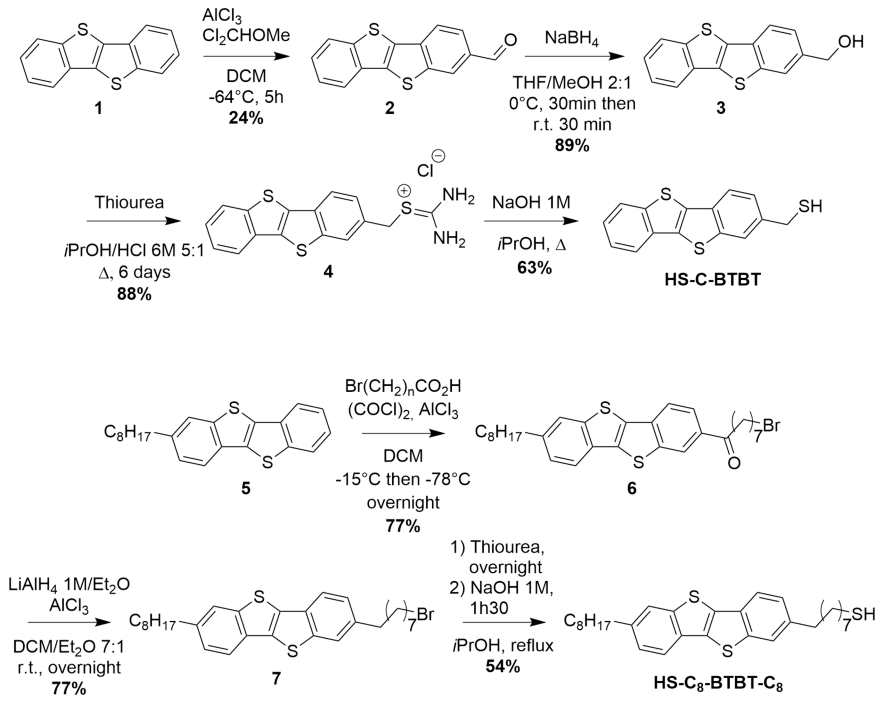

Figure 1. Schemes of the synthesis of HS-C-BTBT and HS-C_8-BTBT-C_8.

recently measured for alkanethiol and OPE MJs (*vide supra*), and makes BTBT derivatives attractive candidates to optimize the thermoelectric figure of merit. The mean electrical conductance (per molecule) is estimated at 2.7×10^{-10} S ($3.5 \times 10^{-6} G_0$, with G_0 being the quantum of conductance $G_0 = 2e^2/h = 77.5\ \mu S$) for the BTBT molecules and is not measurable for the C_8-BTBT-C_8 molecules. Electron transport (ET) properties through the BTBT SAMs reveal a broad distribution of the conductance and of the energy of the molecular orbital involved in the ET. These features are explained by DFT calculations considering several configurations of the molecules in the SAM (tilt and twist angles, packing density). We also calculated at the DFT level the Seebeck coefficients to be $S_{BTBT} \approx 36\ \mu V/K$ and $S_{C8\text{-}BTBT\text{-}C8} \approx 245\ \mu V/K$.

Two molecules were specifically synthesized with very different alkyl chain lengths (see details of the synthesis routes and characterization in the Supporting Information): HS-C-BTBT and HS-C_8-BTBT-C8, where BTBT stands for [1]benzothieno[3,2-*b*][1]benzothiophene (Figure 1). The synthesis of the BTBT analogue bearing a thiol anchor for SAM experiments was first considered by introducing the thiol group directly on the BTBT core. However, this method would probably have led to an unstable material sensitive to oxidation into sulfoxide or sulfone, as it has been previously described by some of us for 2,7-dithio-BTBT.[18] We thus considered synthesizing HS-C-BTBT in 3 steps (Figure 1) starting from the regioselective formylation of BTBT **1** at the second position, as previously described by Košata et al.[19] using modified conditions inspired by a patent from Etori et al.[20] These conditions, although enabling the increase of the regioselectivity of the formylation on the second position over the fourth from 2:1 to 7:1 with respect to Košata's procedure, and reaching a conversion ratio of BTBT of about 89%, gave a yield of only 24% due to the difficulty to isolate all the products by column chromatography. The reduction of aldehyde **2** with sodium tetraborohydride was performed according to a patent of Kawakami and Yamaguchi[21] in good yields. Finally, substitution of the hydroxy group by thiourea followed by its hydrolysis to thiol was performed following the procedure of Cho et al.,[22] affording HS-C-BTBT with a moderate though honorable overall yield of 12% considering the propensity of the compound to dimerize.

The synthesis of HS-C_8-BTBT-C_8 was performed by introducing an end-brominated octyl chain on monooctyl-BTBT **5** in view of introducing the thiol group at the final steps. Synthesis of C8-BTBT **5** was carried out using the conditions previously described,[23] and the introduction of the *η*-bromooctyl chain was performed by Friedel−Crafts reaction using the corresponding carboxylic acids in good yields. Reduction of the corresponding ketones **6** keeping safe the bromine atom was performed using the conditions previously published[24] involving the use of $AlCl_3$ and $LiAlH_4$ 1 M in diethyl ether to afford compound **7** in good yields. Finally, the same substitution-hydrolysis sequence as used for the synthesis of HS-C-BTBT adapted from the work of Cho et al.[22] allowed us to obtain HS-C_8-BTBT-C_8 in a moderate overall yield of 26%.

The SAMs were formed in solution on ultraflat template stripped Au surface (^{TS}Au), and their thicknesses were measured by ellipsometry at 0.9 ± 0.2 nm and 2.6 ± 0.2 nm, in good agreement with the values deduced from geometry optimization of the molecule/^{TS}Au interfaces (see details in the Supporting Information). The topographic AFM images (Figure S1 in the Supporting Information) show that the SAMs are free of gross defects with a rms roughness of 0.6−0.7 nm close to our naked ^{TS}Au substrate (*ca.* 0.4 nm).[25]

The thermal conductivity of the SAMs was measured by the null-point scanning thermal microscope (NP-SThM) method.[26] In brief (see details in the Supporting Information), this is a differential method measuring the tip temperature jump ($T_{NC} - T_C$) when the tip enters in contact with the surface sample, T_{NC} and T_C being the tip temperature just before and after the contact. Starting from a remote position, the heated

https://doi.org/10.1021/acs.jpclett.4c02753
J. Phys. Chem. Lett. 2024, 15, 11593−11600

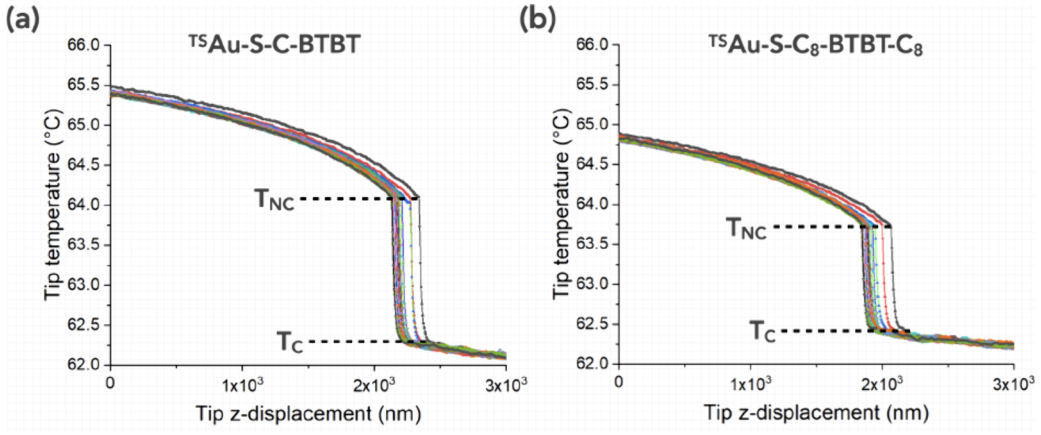

Figure 2. Typical tip temperature vs tip−surface distance measured at V_{WB} = 1.1 V during the approach z-scan (0 corresponds to the tip retracted), 25 traces acquired sequentially at the same location on the SAM: (a) on the ^{TS}Au-S-C-BTBT and (b) on the ^{TS}Au-S-C_8-BTBT-C_8 SAMs.

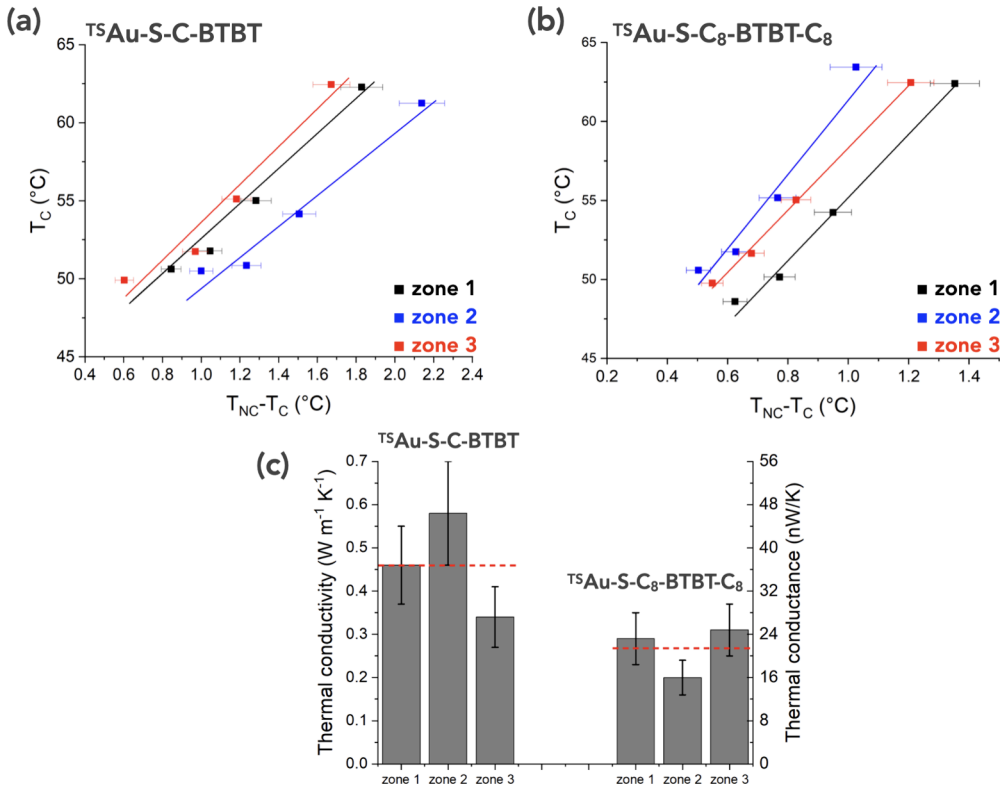

Figure 3. Tip temperature at contact, T_C, versus the temperature jump, $T_{NC} - T_C$, measured at various heating amounts of the tip (T_C increases with the voltage applied on the Wheatstone bridge, V_{WB}= 0.7; 0.8, 0.9, and 1.1 V). The measurements were done at 3 locations (randomly chosen): (a) on the ^{TS}Au-S-C-BTBT and (b) on the ^{TS}Au-S-C_8-BTBT-C_8 SAMs. The lines are linear fits from which the thermal conductivity is determined (eq 1). (c) Thermal conductivity, κ_{SAM}, and thermal conductance, $G_{th,SAM}$, for the three zones of the two MJs. The dashed red lines indicate the mean values (Table 1).

tip approached the surface and the measured tip temperature started decreasing slowly because the heat transfer through the air gap is increased. At contact, the sudden jump from T_{NC} to T_C is due to the additional heat flux passing through the SAM/tip contact. This approach allows removing the parasitic contributions (*e.g.*, air thermal conduction, radiation). Figure 2 shows the typical tip temperature versus tip vertical displacement (25 T_{tip}-z traces per sample) measured on the ^{TS}Au-S-C-BTBT and ^{TS}Au-S-C_8-BTBT-C_8 SAMs. These curves were measured for several heat fluxes passing through the ^{TS}Au-SAM/tip junctions (*i.e.*, by increasing the heating of the tip by increasing the voltage, V_{WB}, applied to the Wheatstone bridge in which the SThM tip is inserted, the substrate being at ambient temperature, see the Supporting Information).

Figure 3 shows the T_C vs ($T_{NC} - T_C$) curves at several heat fluxes for the two samples. The thermal conductivity of the SAM/Au samples, $\kappa_{SAM/Au}$, is calculated from the slope of these curves, according to the relationship:[26]

$$T_C - T_{amb} = \left(\alpha \frac{1}{K_{SAM/Au}} + \beta\right)(T_{NC} - T_C) \quad (1)$$

https://doi.org/10.1021/acs.jpclett.4c02753
J. Phys. Chem. Lett. 2024, 15, 11593−11600

Table 1. Values of the Measured Thermal Conductivity of the SAM/Au Samples, $\kappa_{SAM/Au}$; Thermal Conductivity of the SAM Removing the Au Substrate Contribution, κ_{SAM}, and the Corresponding Thermal Conductance of the SAMs, $G_{th,SAM}$ (See Text)

	^{TS}Au-S-C-BTBT			^{TS}Au-S-C$_8$-BTBT-C$_8$		
	$\kappa_{SAM/Au}$ (W m^{-1} K^{-1})	κ_{SAM} (W m^{-1} K^{-1})	$G_{th,SAM}$ (nW/K)	$\kappa_{SAM/Au}$ (W m^{-1} K^{-1})	κ_{SAM} (W m^{-1} K^{-1})	$G_{th,SAM}$ (nW/K)
zone #1	7.67	0.46 ± 0.08	37 ± 6	1.76	0.29 ± 0.06	23 ± 5
zone #2	9.75	0.58 ± 0.12	46 ± 10	1.23	0.20 ± 0.04	16 ± 3
zone #3	3.71	0.34 ± 0.07	27 ± 5	1.82	0.31 ± 0.06	25 ± 5
mean		0.46 ± 0.09	37 ± 7		0.27 ± 0.05	22 ± 4

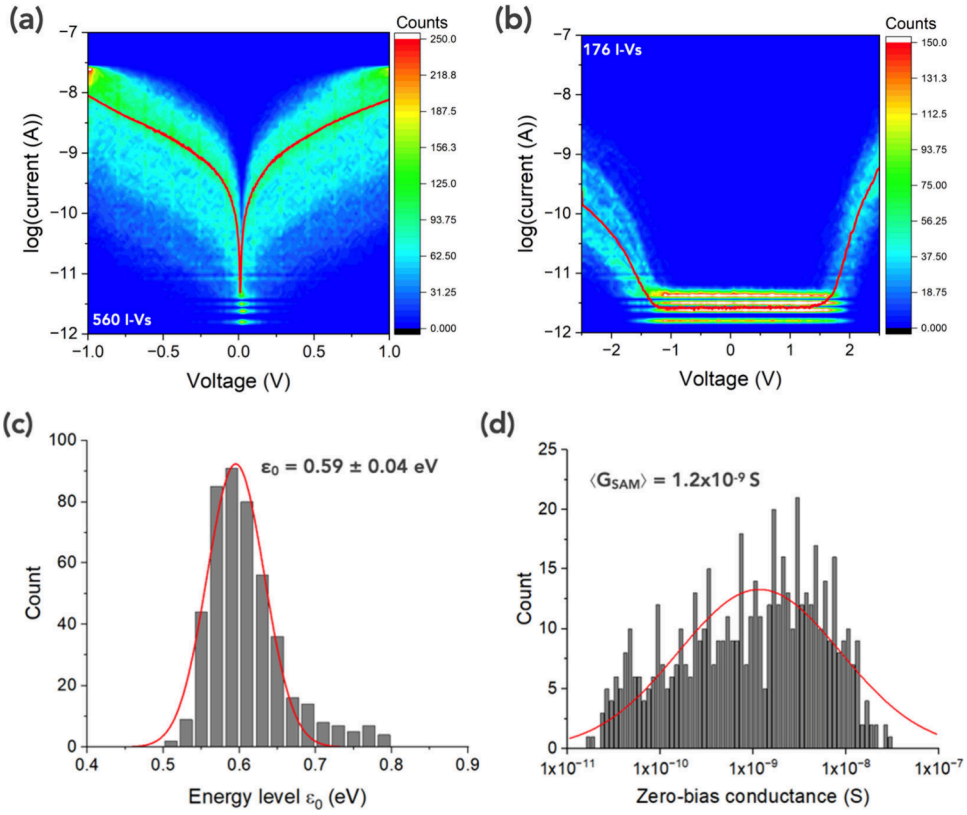

Figure 4. 2D histograms of the I−V curves: (a) ^{TS}Au-S-C-BTBT/PtIr C-AFM tip molecular junctions; (b) ^{TS}Au-S-C$_8$-BTBT-C$_8$/PtIr C-AFM tip molecular junctions. The red lines are the mean I−V curves. (c) Distribution of the energy values ε_0 for the data set of the ^{TS}Au-S-C-BTBT/PtIr C-AFM tip molecular junctions. The solid red line is the fit with a normal distribution with the mean value ± the standard deviation shown in the panel. (d) Statistical distribution of the zero-bias SAM conductance. The red line is a fit by a log-normal distribution with log-mean, log-μ = −8.93 (or mean $\langle G_{SAM}\rangle$ = 1.2 × 10^{-9} S), log standard deviation, log-σ = 0.87.

where α and β are calibration parameters dependent on the tip and equipment. They were systematically measured for all the data shown in Figure 3 (see the Supporting Information), and T_{amb} is the room temperature (22.5 °C in our air-conditioned laboratory). Due to the very weak thickness of the SAMs, the high thermal conductivity of the Au electrode (318 W m^{-1} K^{-1}) contributes to these measured values. The thermal conductivity of the SAM, κ_{SAM}, is obtained by correcting this measured value from the Au electrode contribution using the Dryden model,[27] following the same approach as in our previous work on the thermal conductivity of very thin organic films (<10 nm) of PEDOT:OTf deposited on Au electrode[28] (see also details in the Supporting Information, eq S1). The values of κ_{SAM} are shown on Figure 3c for measurements done on three distinct zones (randomly chosen) for each sample (also summarized in Table 1 with the $\kappa_{SAM/Au}$ values). On average, we obtained $\kappa_{SAM(BTBT)}$ = 0.46 ± 0.27 W m^{-1} K^{-1} and $\kappa_{SAM(C8\text{-}BTBT\text{-}C8)}$ = 0.27 ± 0.16 W m^{-1} K^{-1}. Equivalently, the thermal conductance of the MJs, $G_{th,SAM}$, is given by $G_{th,SAM}$ = $4r_{th}\kappa_{SAM}$ at the thermal constriction between tip and SAM[29] (r_{th} is the thermal contact radius ≈20 nm, see the Supporting Information, eq S2). The mean values are $G_{th,SAM(BTBT)}$ = 37 ± 21 nW/K and $G_{th,SAM(C8\text{-}BTBT\text{-}C8)}$ = 22 ± 13 nW/K.

The electron transport (ET) properties of the same SAMs were also measured by conductive-AFM (details of the measurement protocols and data analysis in the Supporting Information). Figures 4a and 4b show the 2D histograms ("heat map") of the current−voltage (I−V) characteristics measured on the ^{TS}Au-S-C-BTBT/PtIr C-AFM tip and ^{TS}Au-S-C$_8$-BTBT-C$_8$/PtIr C-AFM tip molecular junctions (MJs). Due to the presence of the C8 alkyl chains at the α,ω positions of the BTBT, the conductance of the C$_8$-BTBT-C$_8$ MJs is much lower and no current is measurable in the applied voltage range from −1.5 to 1.5 V (below the sensitivity limit of the C-AFM instrument ≲2−3 pA); this is due to the decrease in the electron transmission probability at the Fermi energy, $T(\varepsilon_F)$, by a factor ≈10^4 (see simulation section). For the BTBT MJs, the I−V data set was analyzed with the single

https://doi.org/10.1021/acs.jpclett.4c02753
J. Phys. Chem. Lett. 2024, 15, 11593−11600

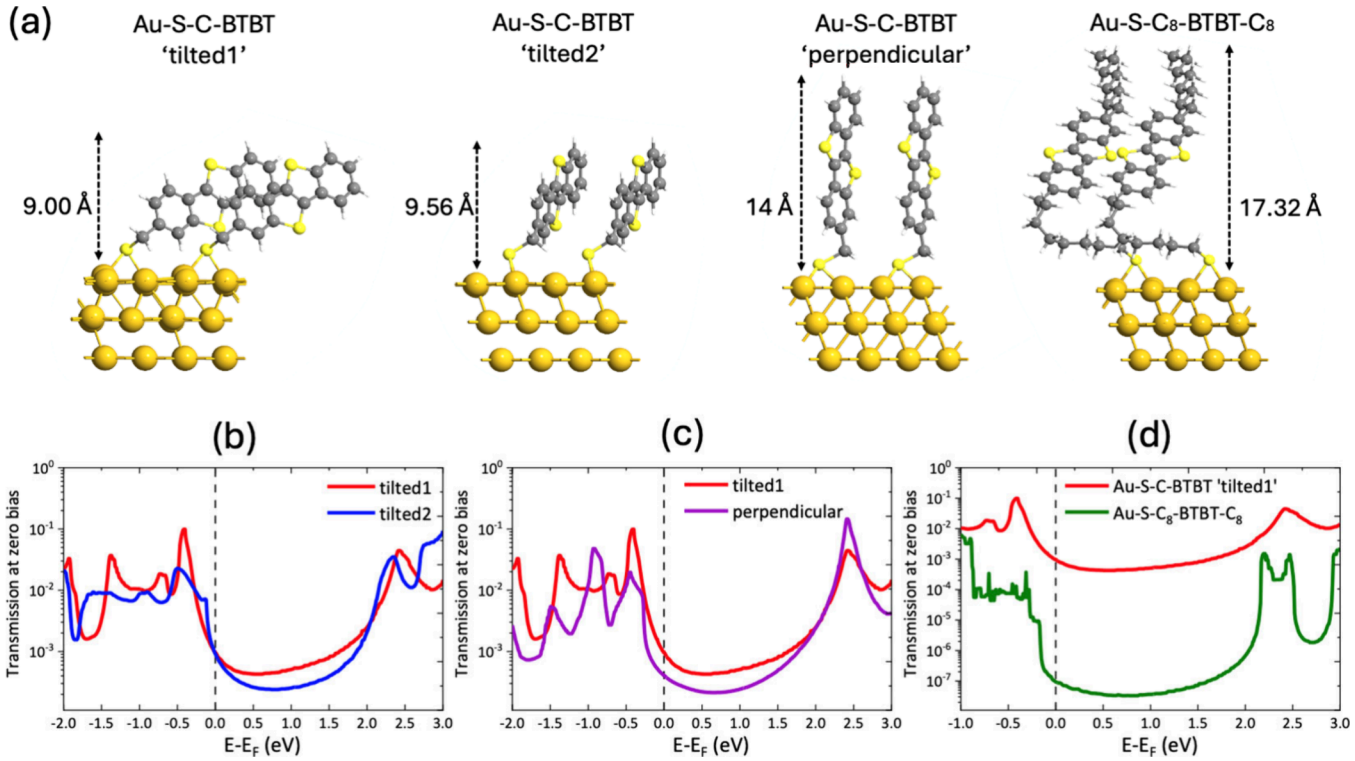

Figure 5. (a) Schemes of the various structural models of Au-molecule SAMs. (b) Calculated transmission coefficient at zero bias for the ^{TS}Au-S-C-BTBT SAM with two configurations for the tilted molecules: the molecule edge toward the Au surface (red line, "tilted1") or the face toward the surface (blue line, "tilted2"). (c) Calculated transmission coefficient at zero bias for the ^{TS}Au-S-C-BTBT SAMs with the maximum packing density (see text) and the molecules perpendicular to the surface (purple line). (d) Comparison of the calculated transmission coefficient at zero bias for the ^{TS}Au-S-C-BTBT MJ ("tilted1" configuration, red line) and for the ^{TS}Au-S-C_8-BTBT-C_8 MJ (green line).

energy-level model (SEL model, eq S6 in the Supporting Information), which gives the energy position ε_0 of the molecular orbital (here the highest occupied molecular orbital, HOMO) involved in the electron transport as well as the electronic coupling energies with the two electrodes Γ_1 and Γ_2 (hybridization between the molecular orbitals and the electron density of states in the electrodes). Figure 4c shows the statistical distributions of the ε_0 parameter obtained by fitting the SEL model on all individual $I-V$ traces of the data set shown in Figure 4a. Note that such an analysis is not possible for the C_8-BTBT-C_8 MJs due to the lack of a measurable current in the −1.5 V/1.5 V window (Figure 4b). The ε_0 statistics show a normal distribution with a main value at ε_0 = 0.59 ± 0.04 eV, with a small tail at higher energy values. The zero-bias conductances of the SAMs (first derivative of the I−Vs in Figure 4a) show a very broad dispersion of the values. It can be fit by a log-normal distribution with a mean conductance value of $\langle G_{SAM} \rangle = 1.2 \times 10^{-9}$ S. A great dispersion is also observable from the statistical distribution of the current at a given voltage (see Figure S4 in the Supporting Information), which is broad with a large tail at lower currents. These experimental behaviors of the conductance/current values result in broadly distributed values of the electrode coupling energies Γ_1 and Γ_2 (0.1 to 10 meV, Figure S5) with the SEL model fits. These features may indicate the existence of several molecular organizations in the SAM and/or configurations at the molecule/SAM interface (*vide infra*, simulations section). Note that the data seems less dispersed for the C_8-BTBT-C_8 MJs (Figure 4b), but it is likely due to the smaller size of the data set, a large fraction of the I−Vs having been discarded because the currents were below the sensitivity limit of the C-AFM equipment (see "data anaylsis" in the Supporting Information).

In order to shed light on the experimental data, we calculated the energy dependent transmission probability, $T(\varepsilon)$, for the two MJs using DFT (density functional theory); see details in the Supporting Information. To explain the broad dispersion of ET in the ^{TS}Au-S-C-BTBT MJ (Figures 4c and 4d), we simulated $T(\varepsilon)$ for several conformations of the BTBT molecule in the SAMs. The structural model of the ^{TS}Au-S-C-BTBT MJ is built by considering tilted molecules with a density of molecules deduced from the ellipsometry measurements (≈ 0.45 nm^2/molecule, see Tables S1). We first considered two conformations, with the molecules tilted with their edge toward the Au surface (referred to as "tilted1") or their aromatic plane toward the surface ("tilted2"), Figure 5a. Indeed, thiolated SAMs planar aromatic rings often organize as ordered domains differing by their organization.[30,31] The calculated $T(\varepsilon)$ shows a small energy difference for the HOMO with respect to the Fermi level (Figure 5b), and the "tilted2" configuration gives a HOMO deeper in energy by 0.1 eV (HOMO at 0.4 eV for "tilted1" and 0.5 eV for "tilted2"). The calculated total energy of the "tilted1" configuration is lower than the one of the "tilted2" configuration by 0.31 eV. The "tilted1" configuration is the most stable and therefore the most probable configuration. We note that, although the calculated energies (0.4 and 0.5 eV, Figure 5b) do not exactly match the experimental values (0.59 eV, Figure 4c), the calculated energy shift between the two matches the 0.2−0.3 eV experimental dispersion. We note that the amplitude of $T(\varepsilon)$ in the energy window −1/+1 eV is different for the two configurations that may contribute to the dispersion of the

https://doi.org/10.1021/acs.jpclett.4c02753
J. Phys. Chem. Lett. 2024, 15, 11593−11600

measured I−V curves, assuming a mix of the two configurations in the SAM.

We also considered another hypothesis. The SAM thickness measurement by ellipsometry gives an average value over a large area (light spot on the order of mm^2), while the C-AFM tip probes a tiny area (≈ 10 nm^2, see the Supporting Information). Therefore, if small clusters of more densely packed molecules are embedded in an overall less dense SAM, the C-AFM data set can include I−V traces recorded on such denser clusters. The coexistence of nanoscale domains with different molecular organization is the consequence of the growth mechanisms of the SAMs.[30,32] We calculated $T(\varepsilon)$ for a SAM at its maximum packing density (≈0.26 nm^2/molecule, Table S1), with the molecules nearly perpendicular to the Au surface (Figure 5c). In that case, the HOMO is only very weakly shifted (at 0.45 eV), but another transmission peak (HOMO−1) with a large amplitude appears close to it (≈0.9 eV), *i.e.*, readily accessible in the energy window used for the I−V measurements. In this case, when the I−V curves in the data set coming from such compact packing clusters are analyzed with the SEL model, the fit likely returns a slightly higher "effective" energy ε_0 value, giving rises to the higher energy tail in the distribution (Figure 4c). The values of $T(\varepsilon)$ in the HOMO−LUMO gap are also different, again contributing to the dispersion of the experimental conductance/current. For the ^{TS}Au-S-C_8-BTBT-C_8 MJs, we calculated $T(\varepsilon)$ considering the same density of molecules as that for the ^{TS}Au-S-C-BTBT MJs, as deduced from the thickness measurements (Table S1). The HOMO lies at about the same energy as for the ^{TS}Au-S-C-BTBT MJs (Figure 5c) and as expected $T(\varepsilon)$ at the Fermi energy is decreased by a factor ≈10^4 in consistency with the decrease in the measured current (>10^3 in the −1 to 1 V window, Figure 4). Finally, from the slope of $T(\varepsilon)$ at the Fermi energy, we calculated the Seebeck coefficient as[1]

$$S = -\frac{\pi^2}{3}\frac{k^2 T}{e}\left(\frac{\partial \ln T(\varepsilon)}{\partial \varepsilon}\right) \quad (2)$$

with k the Boltzmann constant, e the electron charge, T the temperature. Doing so, we obtain $S \approx 36$ and 245 μV/K for the ^{TS}Au-S-C-BTBT (from the calculated $T(\varepsilon)$ of the "tilted1" configuration) and ^{TS}Au-S-C_8-BTBT-C_8 MJs, respectively.

In a simple model, the difference between the thermal resistance of the ^{TS}Au-S-C_8-BTBT-C_8 MJ and the ^{TS}Au-S-C-BTBT MJ is twice the thermal resistance of the C_8 alkyl chain (see the Supporting Information, Figure S6). Given the estimated number of molecules contacted by the SThM tip (∼2500, see Supporting Information), the thermal conductance per molecule deduced from the measurements of $G_{th,SAM}$ (Table 1) are $G_{th,mol} \approx 15$ pW/K for BTBT and ≈8.8 pW/K for C_8-BTBT-C_8, from which we infer a thermal conductance of ≈42 pW/K for the C_8 alkyl chain in our MJs. We note that this crude estimation is fairly of the same order of magnitude as the previously measured values for octane chains in SAM-based MJs (≈ 14 pW/K)[7] and single molecule experiments (≈ 26 pW/K and 37 pW/K).[8,14] This simple estimation assumes that the molecule−electrode interface thermal resistance (interface Kapitza resistance)[33,34] is the same at the covalent bottom interface (Au-S-C−) and at the top molecule/tip interface (−CH_3/Pd SThM tip or −phenyl/Pd SThM tip), which is not rigorously exact since the nature of the molecule-interface matters (covalent vs. van der Waals). It was shown for alkane-based MJs (using time-domain thermal reflectance) that van der Waals molecule−electrode interfaces result in lower thermal conductance than a covalent molecule−electrode interface (by a factor of ∼2).[35] The chemical nature of the electrode metal matters too (*e.g.*, the thermal conductance of Au-alkanedithiol-Au is *ca.* twice that of Au-alkanedithiol-Pd due to interface vibrational mismatch).[36] Nevertheless, this general agreement with previous measurements validates the present data. For completeness, the electronic contribution to the thermal conductance was estimated and, as expected,[37] is negligible. From the C-AFM measurements (Figure 4), the mean electronic conductance per molecule at zero bias is $G_{e,mol} \approx 8 \times 10^{-11}$ S (≈ $1 \times 10^{-6} G_0$, with G_0 the quantum of conductance $G_0 = 2e^2/h = 77.5$ μS) for the ^{TS}Au-S-C-BTBT (considering the mean conductance peak, $G_{e,SAM} = 4.1 \times 10^{-9}$ S, Figure 4c, with ∼15 molecules in the C-AFM MJ, see the Supporting Information). Assuming that the Wiedemann−Franz law holds in MJs and at atomic scale[8,14,38] (which is still an open question at the nanoscale in general),[39,40] we deduced an electronic contribution to the thermal conductance $G_{th,elec} = G_{e,mol} L_0 T = 6 \times 10^{-4}$ pW/K, with L_0 the Lorenz number (2.44×10^{-8} W Ω K^{-2}) and T the temperature. Albeit there is uncertainty in the number of molecules in contact with both the C-AFM and SThM tips, this value of the electronic thermal conductance of BTBT is of the same order of magnitude as the values for molecules like octanethiol and OPE3 (around 0.01 pW/K)[7] or as the smaller and negligible values for many molecules.[8,41]

The thermal conductance of the single molecule (≈15 and ≈8.8 pW/K, for BTBT and C_8-BTBT-C_8, respectively) are on a par or smaller than that of alkyl chains and OPE: 15−30 pW/K (alkanedithiol, 2 to 10 carbon atoms),[8] 10−25 pW/K (alkanethiol, 2 to 18 carbon atoms),[7] ≈37 pW/K (8 carbon atoms),[14] ≈50 pW/K (2 to 24 carbon atoms),[4] and ≈23−24 pW/K for OPE derivatives.[11,14] With a calculated Seebeck coefficient of 36 μV/K and a mean single molecule electrical conductance of 8×10^{-11} S (*vide supra*), we estimate a mean $ZT \approx 2 \times 10^{-6}$ (for BTBT at 300 K). An upper limit can be estimated from the measured statistical distributions: with a maximal electron conduction $G_{e,mol} = 2.5 \times 10^{-9}$ S ($G_{SAM,max} = 3 \times 10^{-8}$ S, Figure 4d), and the lowest thermal conductance $G_{th,mol} \approx 6.4$ pW/K (minimal value of $G_{th,SAM} = 16$ nW/K, Table 1), we can get $ZT_{max} \approx 1.1 \times 10^{-4}$. These values are comparable with the complete thermoelectric characterization of OPE derivative MJs given ZT (at 300 K) ≈ $1.3-2 \times 10^{-5}$.[11] These values fall short compared to some theoretical, optimized, predictions (e.g., values from 3 to 4 have been theoretically predicted for Zn-porphyrin MJs)[42] and the required needs of $ZT > 1$ to envision practical applications.[10,43]

The higher Seebeck coefficient of the C_8-BTBT-C_8 MJ is consistent with a decrease of the electrode coupling energies (due to the intercalation of the C_8 alkyl chains). Such a decrease in the electrode energy coupling is known to reduce the broadening of the molecular orbitals and, thus, to increase the slope of $T(\varepsilon)$ at ε_F. However, in the present case, this also induces a large decrease in electron conductance (Figure 4b). Smaller alkyl chains (say, 3−4 carbon atoms) might be the compromise for not lowering the electronic conductance too much, while maintaining a thermal conductance below 10 pW/K and a Seebeck coefficient above 200 μV/K, these last two conditions being prerequisite to obtain high ZT molecular devices.[10]

https://doi.org/10.1021/acs.jpclett.4c02753
J. Phys. Chem. Lett. 2024, 15, 11593−11600

To sum up, we have combined experiment and theory to characterize the full thermoelectric properties of two benzothieno-benzothiophene (BTBT) SAM-based molecular junctions. We controlled the phononic thermal conductance by inserting alkyl chains (8 carbon atoms) between the BTBT core and the two electrodes. As previously demonstrated in thin films of the same molecules,[17] the alkyl chains efficiently reduced the phononic thermal transport, and the thermal conductance of the C_8-BTBT-C_8 molecular junctions is decreased reaching a low value of 8.8 pW/K (per molecule vs 15 pW/K in the BTBT molecular junction), one of the lowest thermal conductance for molecular junction so far measured.[41] Similarly, the efficient decoupling of the BTBT core from the electrodes leads to one of the highest expected Seebeck coefficient, $S = 245\ \mu V/K$, for a molecular device,[12,13] but at the expense of a too drastic reduction of the electron conductance. Further molecular engineering and optimization are required to avoid this drawback (e.g., shorter alkyl spacers, other anchoring groups, functionalization with side groups).[43] The thermoelectric figure of merit (at 300 K) of the core BTBT molecular junction is determined in a range $ZT \approx 2 \times 10^{-6}$ to 10^{-4}, on a par with the experimental values reported for the archetype molecular junction based on oligo(phenylene ethynylene) derivatives, $ZT \approx 1.3-2 \times 10^{-5}$.[11]

■ ASSOCIATED CONTENT

Supporting Information

The Supporting Information is available free of charge at https://pubs.acs.org/doi/10.1021/acs.jpclett.4c02753.

Details on the molecule synthesis, NMR and MS characterizations, fabrication of the samples (electrodes and SAMs), ellipsometry measurements, topographic AFM and roughness measurements, SThM measurement protocols and substrate correction of the thermal conductivity, C-AFM measurement procedures, data analysis, electron transport analytical model, and DFT computational details (PDF)

■ AUTHOR INFORMATION

Corresponding Author

Dominique Vuillaume − *Institute for Electronics Microelectronics and Nanotechnology (IEMN), CNRS, Villeneuve d'Ascq 59652, France;* orcid.org/0000-0002-3362-1669; Email: dominique.vuillaume@iemn.fr

Authors

Sergio Gonzalez-Casal − *Institute for Electronics Microelectronics and Nanotechnology (IEMN), CNRS, Villeneuve d'Ascq 59652, France*

Rémy Jouclas − *Laboratory of Polymer Chemistry, Université Libre de Bruxelles, Bruxelles 1050, Belgium*

Imane Arbouch − *Laboratory for Chemistry of Novel Materials, University of Mons, Mons 7000, Belgium*

Yves Henri Geerts − *Laboratory of Polymer Chemistry, Université Libre de Bruxelles, Bruxelles 1050, Belgium; International Solvay Institutes of Physics and Chemistry, Université Libre de Bruxelles, Bruxelles 1050, Belgium;* orcid.org/0000-0002-2660-5767

Colin van Dyck − *Theoretical Chemical Physics group, University of Mons, Mons 7000, Belgium;* orcid.org/0000-0003-2853-3821

Jérôme Cornil − *Laboratory for Chemistry of Novel Materials, University of Mons, Mons 7000, Belgium;* orcid.org/0000-0002-5479-4227

Complete contact information is available at: https://pubs.acs.org/10.1021/acs.jpclett.4c02753

Author Contributions

S.G.C. carried out the SThM and C-AFM measurements. R.J. and Y.G. synthesized the molecules, and S.G.C. fabricated the SAMs. I.A., C.v.D., and J.C. performed the theoretical computations. S.G.C. and D.V. analyzed the SThM and C-AFM data. D.V. supervised the project. The manuscript was written by D.V. with the contributions and comments of all the authors. All authors have given approval of the final version of the manuscript.

Notes

The authors declare no competing financial interest.

■ ACKNOWLEDGMENTS

S.G.C. and D.V. acknowledge support from the ANR (# ANR-21-CE30-0065, project HotElo). Y.G. is thankful to the Belgian National Fund for Scientific Research (FNRS) for financial support through research projects Pi-Fast (No T.0072.18), Pi-Chir (No T.0094.22), 2D to 3D (No 30489208), and CHISUB (No 40007495). Financial supports from the Fédération Wallonie-Bruxelles (ARC No 20061) is also acknowledged. The research in Mons is supported by the Belgian National Fund for Scientific Research (FRS-FNRS) via the EOS CHISUB project (No 40007495) and within the Consortium des Équipements de Calcul Intensif − CÉCI (Grant Number U.G.018.18), and by the Walloon Region (LUCIA Tier-1 supercomputer; Grant Number 1910247). J.C. is an FNRS research director.

■ REFERENCES

(1) Paulsson, M.; Datta, S. Thermoelectric effect in molecular electronics. *Phys. Rev. B* **2003**, *67* (2), No. 241403(R).

(2) Craven, G. T.; Nitzan, A. Electron hopping heat transport in molecules. *J. Chem. Phys.* **2023**, *158* (1), 174306.

(3) Wang, R. Y.; Segalman, R. A.; Majumdar, A. Room temperature thermal conductance of alkanedithiol self-assembled monolayers. *Appl. Phys. Lett.* **2006**, *89* (17), 173113.

(4) Wang, Z.; Carter, J. A.; Lagutchev, A.; Koh, Y. K.; Seong, N.-H.; Cahill, D. G.; Dlott, D. D. Ultrafast Flash Thermal Conductance of Molecular Chains. *Science* **2007**, *317* (5839), 787−790.

(5) Luo, T.; Lloyd, J. R. Equilibrium Molecular Dynamics Study of Lattice Thermal Conductivity/Conductance of Au-SAM-Au Junctions. *J. Heat Transfer* **2010**, *132*, 032401.

(6) Duda, J. C.; Saltonstall, C. B.; Norris, P. M.; Hopkins, P. E. Assessment and prediction of thermal transport at solid-self-assembled monolayer junctions. *J. Chem. Phys.* **2011**, *134* (9), 094704.

(7) Meier, T.; Menges, F.; Nirmalraj, P.; Holscher, H.; Riel, H.; Gotsmann, B. Length-dependent thermal transport along molecular chains. *Phys. Rev. Lett.* **2014**, *113* (6), 060801.

(8) Cui, L.; Hur, S.; Akbar, Z. A.; Klockner, J. C.; Jeong, W.; Pauly, F.; Jang, S. Y.; Reddy, P.; Meyhofer, E. Thermal conductance of single-molecule junctions. *Nature* **2019**, *572* (7771), 628−633.

(9) Wang, K.; Meyhofer, E.; Reddy, P. Thermal and Thermoelectric Properties of Molecular Junctions. *Adv. Funct. Mater.* **2020**, *30* (8), 1904534.

(10) Gemma, A.; Gotsmann, B. A roadmap for molecular thermoelectricity. *Nat. Nanotechnol.* **2021**, *16* (12), 1299−1301.

(11) Gemma, A.; Tabatabaei, F.; Drechsler, U.; Zulji, A.; Dekkiche, H.; Mosso, N.; Niehaus, T.; Bryce, M. R.; Merabia, S.; Gotsmann, B.

Full thermoelectric characterization of a single molecule. *Nat. Commun.* **2023**, *14* (1), 3868.
(12) Rincon-Garcia, L.; Evangeli, C.; Rubio-Bollinger, G.; Agrait, N. Thermopower measurements in molecular junctions. *Chem. Soc. Rev.* **2016**, *45* (15), 4285−4306.
(13) Cui, L.; Miao, R.; Jiang, C.; Meyhofer, E.; Reddy, P. Perspective: Thermal and thermoelectric transport in molecular junctions. *J. Chem. Phys.* **2017**, *146* (9), 092201.
(14) Mosso, N.; Sadeghi, H.; Gemma, A.; Sangtarash, S.; Drechsler, U.; Lambert, C.; Gotsmann, B. Thermal Transport through Single-Molecule Junctions. *Nano Lett.* **2019**, *19* (11), 7614−7622.
(15) Schweicher, G.; Lemaur, V.; Niebel, C.; Ruzie, C.; Diao, Y.; Goto, O.; Lee, W. Y.; Kim, Y.; Arlin, J. B.; Karpinska, J.; et al. Bulky end-capped [1]benzothieno[3,2-b]benzothiophenes: reaching high-mobility organic semiconductors by fine tuning of the crystalline solid-state order. *Adv. Mater.* **2015**, *27* (19), 3066−3072.
(16) Tsutsui, Y.; Schweicher, G.; Chattopadhyay, B.; Sakurai, T.; Arlin, J. B.; Ruzie, C.; Aliev, A.; Ciesielski, A.; Colella, S.; Kennedy, A. R.; et al. Unraveling Unprecedented Charge Carrier Mobility through Structure Property Relationship of Four Isomers of Didodecyl[1]-benzothieno[3,2-b][1]benzothiophene. *Adv. Mater.* **2016**, *28* (33), 7106−7114.
(17) Gueye, M. N.; Vercouter, A.; Jouclas, R.; Guerin, D.; Lemaur, V.; Schweicher, G.; Lenfant, S.; Antidormi, A.; Geerts, Y.; Melis, C.; et al. Thermal conductivity of benzothieno-benzothiophene derivatives at the nanoscale. *Nanoscale* **2021**, *13* (6), 3800−3807.
(18) Ruzié, C.; Karpinska, J.; Laurent, A.; Sanguinet, L.; Hunter, S.; Anthopoulos, T. D.; Lemaur, V.; Cornil, J.; Kennedy, A. R.; Fenwick, O.; et al. Design, synthesis, chemical stability, packing, cyclic voltammetry, ionisation potential, and charge transport of [1]-benzothieno[3,2-b][1]benzothiophene derivatives. *J. Mater. Chem. C* **2016**, *4* (22), 4863−4879.
(19) Košata, B.; Kozmík, V.; Svoboda, J. Reactivity of [1]-Benzothieno[3,2-b][1]Benzothiophene - Electrophilic and Metallation Reactions. *Collect. Czech. Chem. Commun.* **2002**, *67* (5), 645−664.
(20) Etori, H.; Hanna, J.; Inagaki, S.; Ishizuka, A.; Mizuguchi, M. *Benzothienobenzothiophene Derivative, Organic Semiconductor Material and Organic Transistor*. JP2017052707A, 2017.
(21) Kawakami, Y.; Yamaguchi, K. *Compound, Pattern Forming Substrate, Coupling Agent, and Pattern Forming Method*. JP2019019092A, 2019.
(22) Cho, S. J.; Kong, G. D.; Park, S.; Park, J.; Byeon, S. E.; Kim, T.; Yoon, H. J. Molecularly Controlled Stark Effect Induces Significant Rectification in Polycyclic-Aromatic-Hydrocarbon-Terminated n-Alkanethiolates. *Nano Lett.* **2019**, *19* (1), 545−553.
(23) Niebel, C.; Kim, Y.; Ruzié, C.; Karpinska, J.; Chattopadhyay, B.; Schweicher, G.; Richard, A.; Lemaur, V.; Olivier, Y.; Cornil, J.; et al. Thienoacene dimers based on the thieno[3,2-b]thiophene moiety: synthesis, characterization and electronic properties. *J. Mater. Chem. C* **2015**, *3* (3), 674−685.
(24) Combe, C. M. S.; Biniek, L.; Schroeder, B. C.; McCulloch, I. Synthesis of [1]benzothieno[3,2-b][1]benzothiophene pendant and norbornene random co-polymers via ring opening metathesis. *J. Mater. Chem. C* **2014**, *2* (3), 538−541.
(25) Mervinetsky, E.; Alshanski, I.; Lenfant, S.; Guerin, D.; Medrano Sandonas, L.; Dianat, A.; Gutierrez, R.; Cuniberti, G.; Hurevich, M.; Yitzchaik, S.; et al. Electron Transport through Self-Assembled Monolayers of Tripeptides. *J. Phys. Chem. C* **2019**, *123* (14), 9600−9608.
(26) Kim, K.; Chung, J.; Hwang, G.; Kwon, O.; Lee, J. S. Quantitative measurement with scanning thermal microscope by preventing the distortion due to the heat transfer through the air. *ACS Nano* **2011**, *5* (11), 8700−8709.
(27) Dryden, J. R. The Effect of a Surface Coating on the Constriction Resistance of a Spot on an Infinite Half-Plane. *Journal of Heat Transfer* **1983**, *105* (2), 408−410.
(28) Kondratenko, K.; Guerin, D.; Wallart, X.; Lenfant, S.; Vuillaume, D. Thermal and electrical cross-plane conductivity at the nanoscale in poly(3,4-ethylenedioxythiophene):trifluoromethanesulfonate thin films. *Nanoscale* **2022**, *14*, 6075.
(29) Carslaw, H. S.; Jaeger, J. C. *Conduction of Heat in Solids*; Oxford University Press: 1959.
(30) Schreiber, F. Structure and growth of self-assembling monolayers. *Prog. Surf. Sci.* **2000**, *65* (5−8), 151−256.
(31) Duwez, A.-S. Exploiting electron spectroscopies to probe the structure and organization of self-assembled monolayers: a review. *J. Electron Spectrosc. Relat. Phenom.* **2004**, *134* (2), 97−138.
(32) Love, J. C.; Estroff, L. A.; Kriebel, J. K.; Nuzzo, R. G.; Whitesides, G. M. Self-assembled monolayers of thiolates on metals as a form of nanotechnology. *Chem. Rev.* **2005**, *105* (4), 1103−1169.
(33) Kapitza, P. L. Heat Transfer and Superfluidity of Helium II. *Phys. Rev.* **1941**, *60* (4), 354−355.
(34) Hu, L.; Zhang, L.; Hu, M.; Wang, J.-S.; Li, B.; Keblinski, P. Phonon interference at self-assembled monolayer interfaces: Molecular dynamics simulations. *Phys. Rev. B* **2010**, *81* (23), 235427.
(35) Losego, M. D.; Grady, M. E.; Sottos, N. R.; Cahill, D. G.; Braun, P. V. Effects of chemical bonding on heat transport across interfaces. *Nat. Mater.* **2012**, *11* (6), 502−506.
(36) Majumdar, S.; Sierra-Suarez, J. A.; Schiffres, S. N.; Ong, W. L.; Higgs, C. F., 3rd; McGaughey, A. J.; Malen, J. A. Vibrational mismatch of metal leads controls thermal conductance of self-assembled monolayer junctions. *Nano Lett.* **2015**, *15* (5), 2985−2991.
(37) Sadeghi, H.; Sangtarash, S.; Lambert, C. J. Oligoyne Molecular Junctions for Efficient Room Temperature Thermoelectric Power Generation. *Nano Lett.* **2015**, *15* (11), 7467−7472.
(38) Mosso, N.; Drechsler, U.; Menges, F.; Nirmalraj, P.; Karg, S.; Riel, H.; Gotsmann, B. Heat transport through atomic contacts. *Nat. Nanotechnol* **2017**, *12* (5), 430−433.
(39) Burkle, M.; Asai, Y. How To Probe the Limits of the Wiedemann-Franz Law at Nanoscale. *Nano Lett.* **2018**, *18* (11), 7358−7361.
(40) Craven, G. T.; Nitzan, A. Wiedemann-Franz Law for Molecular Hopping Transport. *Nano Lett.* **2020**, *20* (2), 989−993.
(41) Noori, M. D.; Sangtarash, S.; Sadeghi, H. The Effect of Anchor Group on the Phonon Thermal Conductance of Single Molecule Junctions. *Applied Sciences* **2021**, *11* (3), 1066.
(42) Noori, M.; Sadeghi, H.; Lambert, C. J. High-performance thermoelectricity in edge-over-edge zinc-porphyrin molecular wires. *Nanoscale* **2017**, *9* (16), 5299−5304.
(43) Gotsmann, B.; Gemma, A.; Segal, D. Quantum phonon transport through channels and molecules—A Perspective. *Appl. Phys. Lett.* **2022**, *120* (16), 160503.

https://doi.org/10.1021/acs.jpclett.4c02753
J. Phys. Chem. Lett. 2024, 15, 11593−11600